China Geology 8 (2025) 540−549

China Geology

Journal homepage: http://chinageology.cgs.cn
https://www.sciencedirect.com/journal/china-geology

Iron-manganese modified corncob biochar for fluoride removal from groundwater: Insights into adsorption mechanisms

Juan-juan Liu[a, b,*], Si-yuan Ma[b], Xin-wen Yang[b], Wang-ying Chen[b], Abdur Rashid[b]

[a] *Key Laboratory of Eco-Geochemistry*, *Ministry of Natural Resources*, *National Research Center for Geoanalysis*, *Beijing* 100037, *China*
[b] *State Key Laboratory of Bio-Geology and Environmental Geology*, *School of Environmental Studies*, *China University of Geosciences*, *Wuhan* 430074, *China*

ARTICLE INFO

Article history:
Received 16 April 2025
Received in revised form 5 May 2025
Accepted 11 June 2025
Available online 20 June 2025

Keywords:
Corncob biochar
Fe–Mn modification
Fe/Mn molar ratio
Pyrolysis temperature
Defluorination
Adsorption mechanisms
Kinetic and isotherm models
Groundwater remediation
Sustainable Development Goals (SDG 6)
Environmental geological survey engineering

ABSTRACT

Biochar, as an efficient, effective, and potential soil improver, has broad application prospects in the field of defluoridation. This study aimed to evaluate the defluoridation potential of iron (Fe) and manganese (Mn) co-modified biochar from groundwater. The varied Fe/Mn molar ratio (2∶1 and 1∶2) modified biochar was prepared by corncob with the pyrolysis temperature of 300°C, 400°C, and 500°C. Batch experiments for fluoride (F^-) removal were performed by corncob biochar before and after Fe–Mn modified. Their composition, structure, and performance were analyzed by multiple characterization techniques to clarify F^- removal mechanisms. Our results indicated that unmodified corncob biochar produced at 400 °C (BC400) exhibited the highest F^- adsorption efficiency (87.3%) among three unmodified samples, attributable to its largest specific surface area (2.55 m^2/g). Notably, F^- removal amounts by Fe-Mn modified BC400 were 2 times higher than BC400. The enhanced F^- removal performance of Fe–Mn modified biochar can be attributed to several mechanisms: (1) the modification produced rougher surface textures, resulting in an increased specific surface area (about 3.50 m^2/g); (2) newly formed Fe–O and Mn–O bonds on the biochar surface facilitated the formation of complexes with F^-; and (3) the adsorption results fitted well with pseudo-second-order and Freundlich models (R^2>0.98), indicating that the removal process involved physicochemical adsorption. These findings demonstrate that Fe–Mn modified biochar is a highly efficient and cost-effective material for F^- remediation and holds significant potential for application in contaminated groundwater and soil systems.

1. Introduction

Fluoride (F^-) is naturally present in host rocks, soils, groundwater, and biological systems (Goswami R and Kumar M, 2018; Corona-Martinez DA et al., 2025). In recent decades, its environmental and health impacts have drawn growing attention due to its toxicity, bioavailability, environmental persistence, and genotoxicity. (Mohan D et al., 2012; Khan BA et al., 2022; Mwadalu R et al., 2025). Fluoride is an important micronutrient that supports dental and bone health. When human exposure to higher F^- contaminated water causes several types of diseases such as dental, and skeletal fluorosis, liver dysfunction, lower intelligence in children, and even cancer (Mohan D et al., 2014; Li FY et al., 2021; Kumar Rakesh et al., 2023). The World Health Organization (WHO) recommends a maximum F^- concentration of 1.5 mg/L in drinking water. However, this limit is exceeded in regions However, F^- levels in various places, including Italy, Mexico, Japan, the United Kingdom, India, Pakistan, China, Tanzania, Kenya, and Thailand (Ali S et al., 2016; Rasool A et al., 2018; Lacson CFZ et al., 2021). In China, over 80 million people are exposed to excessive F^- levels through drinking water (Wan S et al., 2019). To overcome this challenge, efficient, low-cost, and environmental-friendly materials are needed for F^- removal from soil and groundwater (He J et al., 2020; Li J et al., 2023; Ning K et al., 2024). Biochar has emerged as a promising material due to its favorable adsorption properties and environmental sustainability.

Biochar, a by-product of biomass pyrolysis from sources is widely used for resource recovery, F^- removal, and improving soil and water quality (Mei L et al., 2020; Kumar

First author: *E-mail address*: sallyliu2023@126.com (Juan-juan Liu).

* Corresponding author: *E-mail address*: sallyliu2023@126.com (Juan-juan Liu).

Literary editor: Xi-jie Chen
doi:10.31035/cg20250075
2096-5192/© 2025 China Geology Editorial Office.

R. et al., 2023; Girkar M et al., 2024). In recent years, various types of biochar, such as eggshell, chitosan, fruit peels, and rice husks, have been studied for their effectiveness in removing pollutants from water (Liu H et al., 2020; Meilani V et al., 2021; Yang MG et al., 2023; Mahdavi Z et al., 2024; Ning K et al., 2024; Foroutan R et al., 2025). Corn, a major crop in China, produces about 40 million tons annually, making corncob a readily available by-product for biochar. Previous studies have shown that pyrolysis temperature significantly influences the properties of biochar (Sadhu M et al., 2021; Zou CJ et al., 2024). However, higher pyrolysis temperature usually reduces the specific surface area and functional group diversity of biochar, which can negatively affect its adsorption capacity (Gourai M et al., 2023; Yang YZ et al., 2023; Wang J et al., 2025). Therefore, to enhance its efficiency during contaminant removal, optimized modification methods are needed to improve the adsorption performance of biochar post-pyrolysis.

Iron and manganese oxide (or hydroxides) are highly reactive and widely distributed in the environment and Earth's crust (Yin G et al., 2020; Foroutan R et al., 2024; Liu JJ et al., 2025). In fluoride-contaminated soils and groundwater, the redox potential at the surface of corncob biochar may change due to interactions with surrounding redox-active species. Under such conditions, iron and manganese oxides can deposit onto the biochar surface, forming Fe–Mn modified biochar (Mohan D et al., 2014; Dewage NB et al., 2018). Previous studies have demonstrated that Fe- or Mn-modified biochars exhibit high removal efficiency for various heavy metals and pollutants. For instance, Mn oxide-modified biochar has shown strong adsorption capacity for Pb(II) in wastewater (Wang J et al., 2025). Lin L et al. (2017) reported that Fe–Mn modified corn straw biochar enhanced As(Ⅲ) remove compared to raw biochar. Yin G et al. (2020) found that Fe–Mn modified *Pennisetum* straw biochar effectively adsorbed Cd(Ⅱ) from aqueous solutions. Guo J et al. (2019) developed a ternary HA–Fe–Mn loaded rice husk biochar capable of removing both Cd(II) and As(V). Fe–Mn modified biochar derived from branches and durian shells improved Cd(II) adsorption in water and alkaline soils (Yang T et al., 2022), while while Fe–Mn modified tea branch biochar was effective in stabilizing Sb(III) and Cd(II) in co-contaminated soil (Wang Y et al., 2019). Although biochar is recognized as a cost-effective and environmentally friendly adsorbent for F^- remediation, the F^- adsorption capacity of unmodified biochar remains limited. As F^- can be strongly adsorbed onto the surface of iron (hydroxide) or manganese oxides (Mahdavi Z et al., 2024; Corona-Martinez DA et al., 2025), Fe–Mn modification presents a promising strategy to enhance F^- adsorption. However, few studies have investigated the use of Fe–Mn modified biochar for F^- removal in soil and groundwater, and the underlying removal mechanisms remain unclear.

The main objective of this study was to investigate fluoride (F^-) enrichment in groundwater, and to evaluate the potential of Fe–Mn oxides co-modified corncob biochar for F^- remediation. The study aims were considering as follows: (1) to assess the effect of pyrolysis temperature (300, 400, and 500°C) on the F^- removal efficiency of corncob biochar before and after Fe–Mn modification; (2) to synthesize Fe–Mn modified biochars with different Fe/Mn molar ratios (2∶1 and 1∶2, denoted as BCF_2M_1 and BCF_1M_2, respectively) using BC400 as the base, and compare their defluoridation performance; (3) to analyze the adsorption kinetics (Pseudo-first-order and the Pseudo-second-order models), adsorption isotherms (Langmuir and Freundlich models), and characterize biochars using multiple technologies to clarify the defluoridation mechanism. This study contributes to developing an effective, low-cost strategy for minimizing F^- contamination in groundwater and soil using modified agricultural waste-derived biochar.

2. Materials and methods

2.1. Materials and chemicals

Manganese chloride ($MnCl_2·4H_2O$, MW = 197.9 g/mol, 99%), ferric chloride ($FeCl_3·6H_2O$, MW=270.3 g/mol, 99%), ethylene glycol ($(CH_2OH)_2$, MW = 62.08 g/mol, 98%), sodium acetate (CH_3COONa, MW = 82.03 g/mol, 99%), polyethylene glycol (PEG-600) and urea (CH_4N_2O, MW = 60.06 g/mol, 99%) were used for preparation and modification of corncob biochar. Sodium citrate ($Na_3C_6H_5O_7·2H_2O$, MW = 258.07 g/mol, 99%), potassium nitrate (KNO_3, MW = 101.1 g/mol, 99%) and nitric acid (HNO_3, MW = 63 g/mol, 68%) were required to prepare total ionic strength adjustment buffer (TISAB). And sodium fluoride (NaF) was used as a source compound for F^- standard solution. All chemicals used were analytical grade, which supplied by Sinopharm Chemical Reagent Co., Ltd, China. The ultra-pure water (resistivity > 18.2 MΩ.cm) was used to prepare standard solutions and other dilutions.

2.2. Synthesis and modification of Biochar

Corncob biochar synthesized methods were according to previous studies (Montero JIZ et al., 2018; Wang BL et al., 2024). Firstly, fresh corncobs were collected from local markets (Wuhan City, Hubei, China), then were washed with deionized water for several times to remove impurities. Secondly, corncobs were dried completely at 105°C for 24 h, then ground diameter around 1 cm. Thirdly, the ground corncobs were placed into a ceramic crucible using a quartz tube furnace, and were heated to 300°C, 400°C, and 500°C, respectively, under a nitrogen gas environment for 1 h, with the heating rate set at 5°C/min to facilitate carbonization. After corncob biochar cool at room temperature and grind up to 100 mm mesh. Finally, corncob biochar was washed with deionized water several times and dried at 60°C. The corncobs synthesized under different pyrolysis temperatures were labeled as BC300, BC400, and BC500, respectively.

Here, modification of corncobs biochar was selected at 400°C (BC400) with different Fe/Mn molar ratios followed

previous methods (Yang T et al., 2022). $FeCl_3$ ∶ $MnCl_2$ (2 ∶ 1 or 1 ∶ 2) were dissolved with 40 mL ethylene glycol $(CH_2OH)_2$ and stirred with a magnetic stirrer at room temperature (25°C). Then, 4 g BC400, 3.6 g CH_3COONa, 1.0 g polyethylene glycol (PEG-600), and 2.0 g CH_4N_2O were added successively under the continuous stirring condition for 6 h, followed by filtration and drying at 60°C. The above drying samples were placed in a quartz tube furnace with 5°C/min heating rate and kept constant at 200°C for 1 h under a nitrogen gas environment, after cooling at room temperature, washed with ultra-pure water and dried at 60°C after filtration. Finally, Fe and Mn modified biochar are labeled as BCF_2M_1 and BCF_1M_2 based on their molar ratio.

2.3. Batch adsorption experiment for fluorine removal

To determine the effect of pyrolysis temperatures (300°C, 400°C, and 500°C) of corncob biochar on F^- remediation. Thus, we synthesized corncob biochar BC300, BC400, and BC500 for batch experiments. To evaluate the effect of Fe/Mn molar ratio (2:1 and 1:2,) on corncob biochar modification for F^- removal, we compare corncob biochar before (BC400) and after modification (BCF_2M_1 and BCF_1M_2) for the batch test. For five different corncobs biochar (BC300, BC400, BC500, BCF_2M_1, and BCF_1M_2), both isotherm and kinetic adsorption experiments were considered as follows:

The isotherm experiment was performed to evaluate the effect of initial F^- concentration. At first, 0.10 g of corncob biochar was added into 20.0 mL NaF solution at room temperature (25°C) and was completely mixed on a reciprocal shaker at 150 rpm for 24 h. The concentrations of F^- in solutions were 1 mg/L, 2 mg/L, 5 mg/L, 10 mg/L, and 20 mg/L. After the adsorption of F^- on corncob biochar reached equilibrium, each sample was filtrated using a 0.45 μm membrane filter, then measure F^- concentration by fluoride ion-selective electrode. More details for the measurement and calculation of F^- concentration in the solution can be found in Section 2.4.

The kinetic experiment was done to determine the effect of contact time. Firstly, weight 0.10 g of corncob biochar into 50 mL polyethylene plastic centrifuge tube. Then, 20 mL NaF solution was added with F^- concentration of 20 mg/L at room temperature (25°C), and were completely mixed on a reciprocal shaker at 150 rpm for different time intervals (20 min, 30 min, 60 min, 120 min, 240 min, 480 min, 720 min, and 1440 min). Finally, each sample was filtrated using a 0.45 μm membrane filter, then measure F^- concentration. All experiments were conducted in triplicate at 25°C and the removal concentrations of F^- were calculated.

For investigation of the defluoridation mechanism of varied corncob biochar, Langmuir, and Freundlich isotherms were used to explore the adsorption mechanism based on the data of the isotherm experiment (Langmuir I, 1917; Freundlich, 1926; Li YX et al., 2023). Meanwhile, Pseudo-first-order and Pseudo-second-order models were used fitting parameters based on the results of the kinetic experiment (Ho YS, 2006; Liu J et al., 2016). Equations of these models we used are shown in supporting information (Text S1 and Text S2).

The adsorption capacity of F^- (q_e, mg/g) and removal rate of F^- (R, %) onto corncob biochar were calculated by the following equations (Eq. 1–2).

$$q_e = \frac{(C_0 - C_t) \times V}{m} \tag{1}$$

$$R(\%) = \frac{(C_0 - C_e)}{C_0} \times 100\% \tag{2}$$

Where q_e gives the adsorption capacity of F^- on corncobs biochar, (mg/g); C_t is the concentration of F^- in solution under varied adsorbed times, (mg/L); C_0 and C_e refer to the initial and equilibrium concentration of F^-, (mg/L); V is the volume of F^- solution for reaction, (L); and m refers to the amount of biochar we added, (g).

2.4. Calculation of fluorine concentration

The determination of F^- concentration refers to the water quality determination of the fluoride-ion selective electrode method (GB7484-1987, 1987). The main reagents used in this method are total ionic strength regulator (TISAB), standard F^- storage solution (100 mg/L), and standard F^- solution (10 mg/L). For each test, the different fluorine concentrations should be provisionally configured to draw the curve.

Standard curve drawing: 1 mL, 3 mL, 5 mL, 10 mL, and 20 mL F^- standard solutions were absorbed with a pipetting gun, placed in 50 mL volumetric flask, added 10 mL TISAB, diluted with pure water to the line, shaken well, poured into 150 mL polyethylene cup and put into a magnetic stirring rotor with the solution was continuously stirred. The electrode was inserted in order from low to high concentration. After the potential was stabilized, the potential value was read when the stirring continued. Before each measurement, the electrode should be washed with pure water and dried with filter paper. The measured data should be processed, and the standard curve should be drawn with the potential value as the abscissa and the log value of the concentration as the ordinate.

The determination steps are as follows: 10 mL samples were transferred into a 50 mL volumetric flask with pipetting gun, added 10 mL TISAB, diluted with pure water to the line, shaken well, poured into 150 mL polyethylene beaker, put into a magnetic stirring rotor and inserted electrode with the solution was continuously stirred. Reading the potential value after potential stabilized. Before each measurement, the electrode should be washed with pure water and dried with filter paper. The fluorine ion concentration was calculated according to the potential value of the sample and the standard curve.

2.5. Instrumental characterization

A series of characterization methods were used to evaluate the possible adsorption mechanisms of F^- by corncob biochar and the Fe–Mn modified biochar. The Brunauer-Emmett-

Teller method (BET, ASAP2460, Micromeritics, USA) was applied to determine the surface area, and pore size, and pore size distribution of biochar before and after Fe–Mn modification. Scanning electron microscopy with an energy dispersive spectrometer (SEM–EDS, SU8010, Hitachi, Japan) was used to observe the surface morphology of BC400 and BCF_2M_1 biochar and perform the elemental semi-quantification. Fourier transform infrared spectrometer (FTIR, Nicolet 6700, Thermo Scientific, USA) was carried out for identifying the characteristic surface functional groups present in BCF_2M_1 biochar before and after the adsorption of F^-. X-ray diffractometer (XRD, D8-Focus, Bruker, Germany) was used to analyze the mineral composition and crystal structure of BC400 and BCF_2M_1 biochar, as well as BCF_2M_1 after the adsorption of F^-.

3. Result and discussion

3.1. Characterization of corncob biochar

The characterization of corncob biochar involved measuring surface area, pore structure, morphology, and element distribution. BET and SEM–EDS analyses were conducted to evaluate changes before and after Fe–Mn modification and to assess their influence on F^- adsorption capacity.

Surface area, pore volume, and average pore diameter were measured for biochars produced at different pyrolysis temperatures (BC300, BC400, BC500) and for Fe–Mn modified biochar (BCF_2M_1 and BCF_1M_2), as shown in Table 1. The specific surface areas and pore volume of pyrolysis temperatures treated corncob biochar from large to small in the order: BC400 > BC500 > BC300, which indicated BC400 may shows the highest adsorption capacity of F^- (Table 1). This trend suggests that moderate pyrolysis temperatures enhance porosity, consistent with previous findings (Kumar Rakesh et al., 2023). Following Fe–Mn modification, surface areas increased to 3.50 m^2/g for BCF_1M_2 and 3.76 m^2/g for BCF_2M_1. Both modified biochars also showed higher pore volumes and average pore diameters compared to BC400. These enhancements are attributed to the activation effect of Fe–Mn coatings, which improve the pore structure and provide additional active sites for F^- adsorption (Yin G et al., 2020).

To investigate the morphology and elemental distribution of corncob biochar before (BC400) and after Fe–Mn modification (BCF_2M_1), SEM–EDS analysis was conducted to describe their characterizations. SEM images in Fig. 1 illustrate the morphological differences between BC400 (Figs. 1a–b) and BCF_2M_1 (Figs. 1c–d) at different magnifications. Fig. 1(a) shows that BC400 consisted of irregular particles with varied sizes and morphologies, including retained tubular and layered structures. Some tubular features had collapsed, forming layered porous carbon structures. As shown in Fig. 1(b), the surface of BC400 was relatively smooth and dense, with uniform pore distribution ranging from 1 μm to 4 μm and well-defined pore structures. In contrast, Fig. 1(c) reveals that BCF_2M_1 exhibited a rougher

Table 1. BET results of pyrolysis temperature treated corncob biochar and the Fe–Mn modified biochar.

Samples	BET surface area/(m^2/g)	Pore volume/(cm^3/g)	Average pore diameter/nm
BC300	1.21	0.00078	1.80
BC400	2.55	0.0020	3.17
BC500	2.08	0.0011	2.85
BCF_2M_1	3.50	0.010	11.00
BCF_1M_2	3.76	0.005	5.56

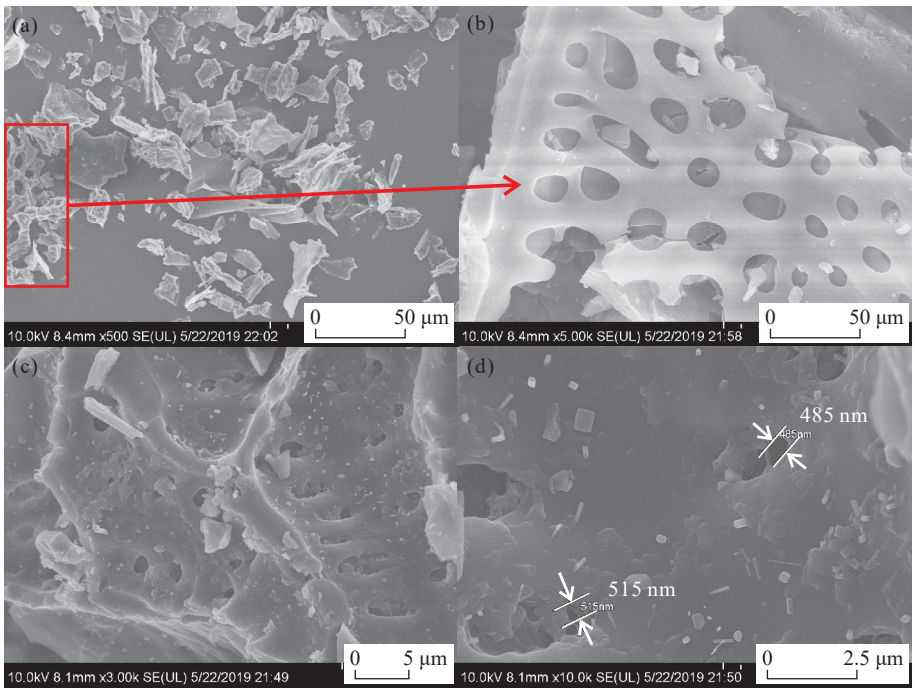

Fig. 1. SEM images of BC400 at ×500 (a); ×5000 (b); and BCF_2M_1 at ×3000 (c); ×10000 (d).

surface with more complex and irregular pore structures, enhancing its physical adsorption capacity (Sadhu M et al., 2021; Mwadalu R et al., 2025). This observation aligns with BET results. Additionally, Fig. 1(d) shows the presence of irregular, needle-like particles (400–700 nm) on the surface of BCF_2M_1, attributed to the deposition of Fe–Mn oxides.

Meanwhile, EDS analysis (as shown in Supporting Information Fig. S1 and Table S1), revealed that the surface of BC400 primarily contained carbon and oxygen, while Fe and Mn were clearly detected on BCF_2M_1, confirming the successful synthesis of Fe–Mn modified corncob biochar. Notably, no aggregated metal oxide particles were observed, suggesting a uniform dispersion of Fe and Mn, which is conducive to increasing the adsorption site and improving the adsorption capacity of corncob biochar. Compared to BC400, the atomic percentage of carbon in BCF_2M_1 decreased from 77.80% to 70.39%, while Fe and Mn increased to 4.18% and 1.65%, respectively. This shift indicates that Fe and Mn partially replaced surface carbon, forming active sites for fluoride binding (Sadhu M et al., 2021; Ning K et al., 2024). Additionally, the increased presence of oxygen-containing functional groups on the modified biochar surface further supports its improved defluoridation performance.

3.2. Effect of pyrolysis temperature for fluorine removal

The effect of pyrolysis temperature (300°C, 400°C, and 500°C) on the adsorption performance of corncob biochar was investigated. Batch adsorption experiments were conducted under varying initial F^- concentrations (1 mg/L, 2 mg/L, 5 mg/L, 10 mg/L, and 20 mg/L). The adsorption capacity and removal efficiency of F^- for BC300, BC400, and BC500 are presented in Fig. 2.

As shown in Fig. 2, the adsorption capacity of F^- on BC300, BC400, and BC500 increased with rising initial F^- concentrations (1–20 mg/L). For BC400 (orange color), the removal rate increased from 61.4% to 87.8%, while the adsorption capacity (q_e) rose from 0.061 to 1.76 mg/g as the initial concentration increased. BC400 and BC500 showed similar adsorption performance, with maximum removal efficiencies of 87.8% and 87.3%, respectively, at 20 mg/L, and BC300 reached 86.2% under the same condition. When comparing the three biochars under identical F^- concentrations, BC400 consistently showed superior adsorption efficiency, aligning with its higher specific surface area and pore volume (Table 1). Based on these results, BC400 was selected for Fe–Mn modification in subsequent experiments.

3.3. Effect of initial concentration for fluorine removal

Under varying initial concentrations of F^- (1 mol/L to 20 mol/L), Fig. 3 illustrates the adsorption capacity and removal efficiency of F^- by BC400 before and after Fe–Mn modification (BCF_2M_1 and BCF_1M_2). In all treatments, adsorption capacity of F^- increased with rising F^- initial concentration. Notably, Fe–Mn modification significantly enhanced fluoride adsorption, especially at concentrations above 5 mg/L, where removal rates exceeded 90%. These findings were consistent with the studies of Lin L et al. (2017), who have reported that Fe–Mn modified corn straw biochar presented greater adsorption of As(III) than corn straw biochar. Moreover, the improved performance in this study can be attributed to the modification process: unmodified BC400 carries a negatively charged surface post-pyrolysis, which limits anion adsorption due to electrostatic repulsion (Yin G et al., 2020; Yang T et al., 2022). Under the same initial concentration of F^-, the adsorption capacity of F^- by Fe–Mn modified BC400 were significantly improved 2 times higher than BC400. This was also consistent with our BET results (Table 1), the specific surface area of BC400 was increased around 1.5 times after modified by Fe–Mn. Thus, Fe–Mn modification effectively enhanced the adsorption capacity of F^- by increasing surface area, pore structure, and available active sites.

Besides, there is no significate difference was observed between BCF_2M_1 and BCF_1M_2 in terms of F^- adsorption, indicating that both Fe/Mn ratios (2∶1 and 1∶2) effectively

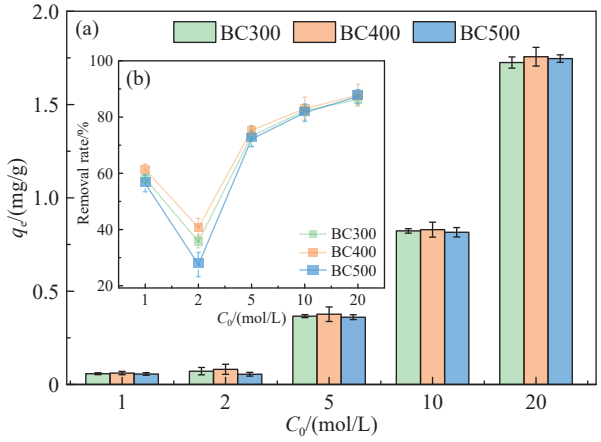

Fig. 2. Adsorption capacity (a) and removal rate (b) of F^- on biochar BC300, BC400, and BC500 under different initial concentration of F^- (1–20 mol/L).

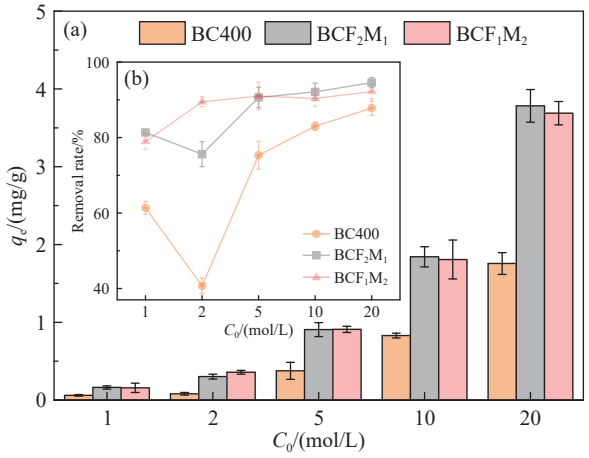

Fig. 3. Adsorption capacity (a) and removal rate (b) of F^- on biochar BC400, BCF_2M_1, and BCF_1M_2 under different initial concentration of fluoride (1–20 mol/L).

enhanced defluoridation. In this study, BCF_2M_1 was selected for further analysis, as iron is generally more abundant than manganese in soils and sediments (Cheng J et al., 2019). With increasing initial F^- concentrations (1.0 mol/L to 20.0 mg/L), the adsorption capacity of BCF_2M_1 increased markedly from 0.16 mg/g to 3.78 mg/g. In contrast, the removal efficiency rose more gradually, from 81.3% to 94.6%. These results confirm that Fe–Mn modification significantly improved the fluoride removal performance of corncob biochar, and both Fe/Mn ratios tested contributed effectively to this enhancement.

3.4. Mechanism of corncob biochar removal fluoride after Fe–Mn modification

3.4.1. Adsorption kinetic models

The effects of contact time on the adsorption of F^- by unmodified (BC400) and Fe–Mn modified corncob biochar (BCF_2M_1) is presented in Fig. 4. As contact time increased, the F^- adsorption capacity of both BC400 (Fig. 4a) and BCF_2M_1 (Fig. 4b) was increased. Notably, the adsorption capacity of F^- on BCF_2M_1 at different contact times (q_t) was much higher than that on BC400, indicating that Fe–Mn modification enhanced the adsorption performance.

The adsorption kinetic behaviors of F^- onto biochar can be divided into two-stage process. In the initial phase (< 200 min), the adsorption capacity increased rapidly due to the abundance of available active sites. In the second phase (> 200 min), with the increase of time, the adsorption capacity continued to increasing slightly and reached to equilibrium around 1440 min. Finally, an adsorption equilibrium was achieved due to saturation of active sites on biochar, and the adsorption and desorption rates remain constant.

Meanwhile, the kinetic data results were fitted to both pseudo-first-order and pseudo-second-order models, with the corresponding parameters were summarized in Table 2. The model fitting results help clarify the adsorption mechanism and rate-controlling steps involved in the fluoride removal process.

Both the pseudo-first-order and pseudo-second-order kinetic models showed high coefficient of determination (R^2 > 0.95), indicating these two models were efficient and effective in describing the adsorption process of F^- onto both BC400 and BCF_2M_1. This suggests that the adsorption process is governed by a combination of physical adsorption on the biochar surface and chemisorption within its structure (Kumar R. et al., 2023; Hota A et al., 2024).

3.4.2. Adsorption isotherm models

To evaluate the interaction between F^- and corncob biochar, adsorption isotherms were examined under varying initial fluoride concentrations (1–20 mg/L) using the Langmuir and Freundlich models. Detailed descriptions of the isotherm models are provided in the Supporting Information (Text S2). Biochars produced at different pyrolysis temperatures (BC300, BC400, and BC500) and Fe–Mn modified variants (BCF_2M_1 and BCF_1M_2) were investigated. The corresponding isotherm parameters of F^- adsorption on corncob biochar are summarized in Table 3.

As shown in Table 3, the adsorption equilibrium data for BC300, BC400, and BC500 were better described by the Langmuir model, with higher R^2 values ranging from 0.934 to 0.965. This suggests that F^- adsorption onto these biochars primarily involved homogeneous monolayer physical or chemical adsorption (Liu JJ et al., 2016; Hota A et al., 2024). Besides, BC400 exhibited the highest Langmuir constant (K_L = 0.044 L/mg), indicating superior adsorption capacity compared to BC300 and BC500. For Fe-Mn modified biochars (BCF_2M_1 and BCF_1M_2), both Langmuir and Freundlich models showed excellent fits (R^2 > 0.98), indicating a combination of homogeneous monolayer and heterogeneous multilayer physicochemical adsorption. The Freundlich constant (K_f), reflecting adsorption capacity, was higher for BCF_2M_1 (3.13 $mg^{1-1/n}\cdot L^{1/n}\cdot g^{-1}$) than for BCF_1M_2 (1.98 $mg^{1-1/n}\cdot L^{1/n}\cdot g^{-1}$). Thus, the adsorption capacity of F^- on BCF_2M_1 would be much better than that on BCF_1M_2. These results validate the successful coating of Fe–Mn oxides on corncob biochar and their role in enhancing fluoride adsorption via surface heterogeneity.

The Langmuir isotherm model for corncob is presented in Fig. 5. As the initial F^- concentration increased, the

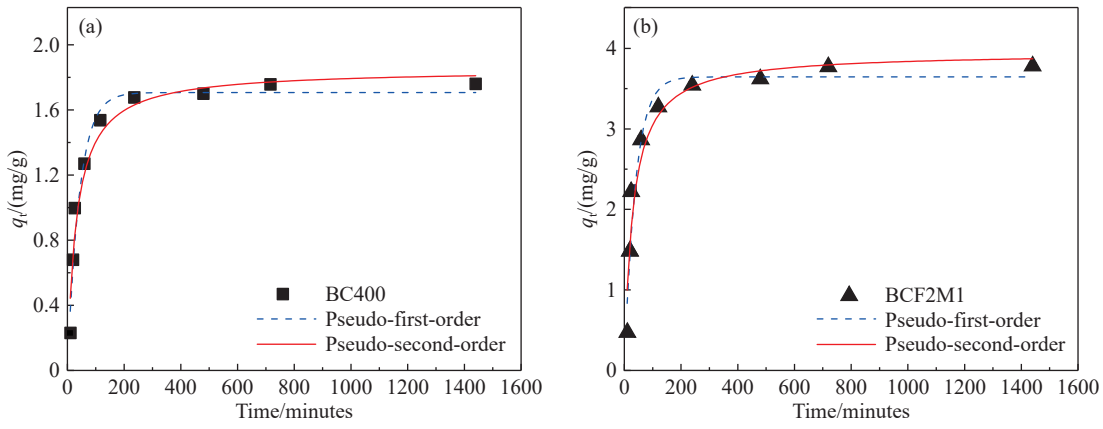

Fig. 4. Adsorption kinetic curve of F^- on corncob biochar BC400 (a), and BCF_2M_1 (b). The dashed and solid curves fitting using pseudo-first-order and pseudo-second-order models, respectively.

adsorption capacity of the biochar also increased, consistent with previous findings (Borno ML et al., 2018). However, the adsorption equilibrium was not fully achieved at concentrations below 20 mg/L may due to insufficient initial F^- levels.

Table 2. Parameters of kinetic models for removal of F^- by corncob biochar.

Samples	Pseudo-first-order			Pseudo-second-order		
	$q_{e,}$ /(mg/g)	k_1 /(1/min)	R^2	$q_{e,}$ /(mg/g)	k_2 /(1/min)	R^2
BC400	1.76	0.024	0.968	1.85	0.017	0.977
BCF_2M_1	3.64	0.02	0.953	3.95	0.01	0.968

Table 3. Parameters of Langmuir and Freundlich isotherm models for removal of F^- by corncob biochar.

Samples	Langmuir			Freundlich		
	q_m/ (mg/g)	K_L /(L/mg)	R^2	K_f/($mg^{1-1/n}$. $L^{1/n}.g^{-1}$)	1/n	R^2
BC300	1.88	0.026	0.965	0.225	1.80	−1.73
BC400	2.30	0.044	0.964	0.0287	1.80	−2.76
BC500	2.06	0.010	0.934	1.45	1.79	−2.83
BCF_2M_1	2020.1	0.0015	0.980	3.13	1.63	0.993
BCF_1M_2	1214.9	0.0017	0.981	1.98	1.35	0.984

3.4.3. Characterization after adsorbed fluoride

To evaluate defluorination efficiency, understanding the sorption mechanism of F^- on corncob biochar is essential. In this study, we characterized corncob biochar before modification (BC400), after Fe–Mn modification (BCF_2M_1), after adsorbed F^- (BCF_2M_1-F) using Fourier-transform infrared spectroscopy (FTIR) and X-ray diffraction (XRD) analyses. Here, FTIR spectra of BC400, BCF_2M_1, and BCF_2M_1-F are shown in Fig. 6, revealing the presence of various functional groups on the biochar surfaces.

The FTIR spectra of the three biochar samples revealed common absorption peaks at 3420 cm^{-1} (–OH stretching), 1615 cm^{-1} (aromatic C=C and C=O bending), and 1440 cm^{-1} (–CH_3 stretching), consistent with previous studies (Kumar R. et al., 2023; Mwadalu R et al., 2025). In BCF_2M_1 and BCF_2M_1-F, an additional peak at 1270 cm^{-1} was observed, attributed to aromatic C–O and phenolic –OH vibrations (Khan BA et al., 2022; Mahdavi Z et al., 2024). Meanwhile, Two further peaks at 537 cm^{-1} and 420 cm^{-1}, corresponding to Fe–O and Mn–O bonds in BCF_2M_1, confirmed the

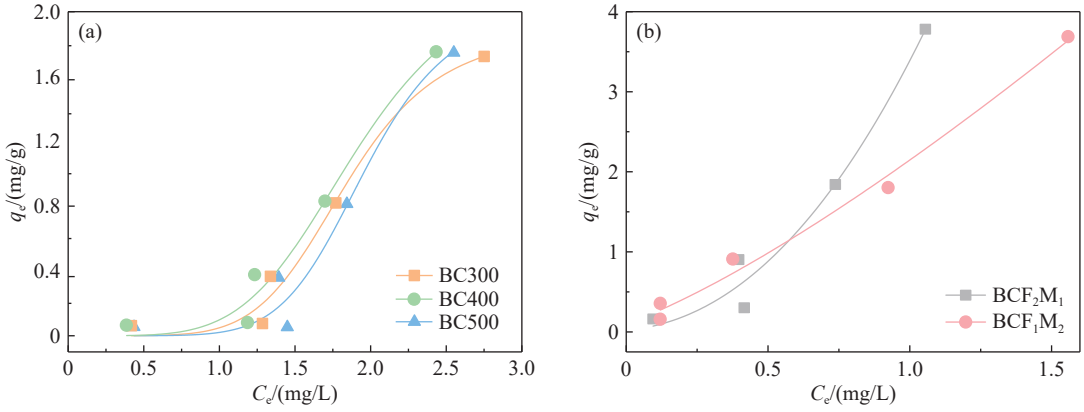

Fig. 5. Langmuir isotherm of F^- by the pyrolysis temperature treated corncob biochar (a) and the Fe-Mn modified biochar (b).

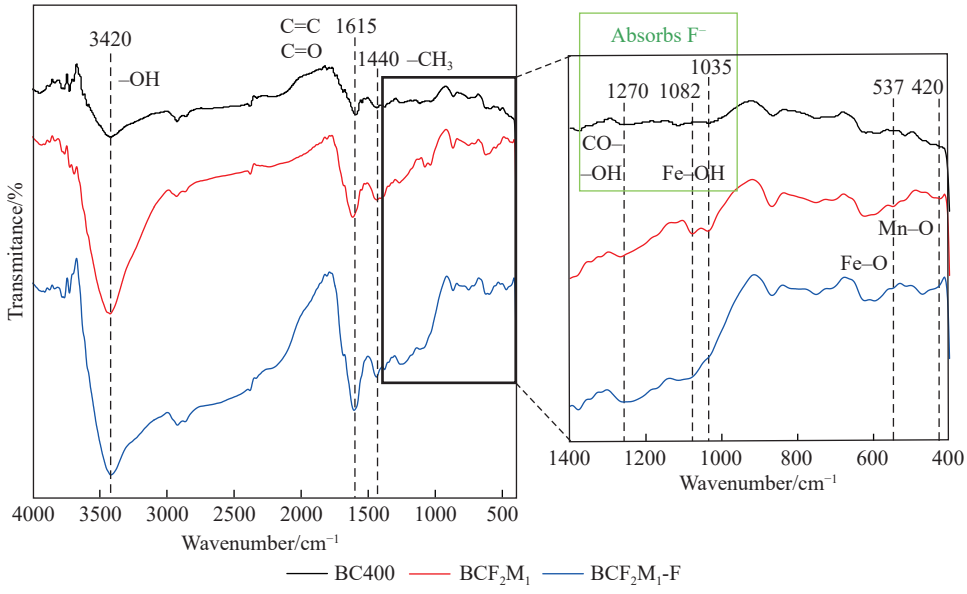

Fig. 6. FTIR spectra of BC400, BCF_2M_1 and BCF_2M_1 after F^- adsorption (BCF_2M_1-F).

successful coating of Fe–Mn oxides on the biochar surface (Foroutan R et al., 2024; Wang J et al., 2025). Besides, BCF_2M_1-F exhibited two stretching vibrations at 1035 cm^{-1} and 1082 cm^{-1}, attributed to Fe–OH groups (Foroutan R et al., 2024; Fu C et al., 2024). The weakening or disappearance of these peaks after F^- adsorption indicates that hydroxyl groups were replaced by F^-. This suggests that –OH groups on Fe–Mn modified biochar participate in ion exchange with F^-, while Fe–O and Mn–O bonds contribute to complex formation, enhancing fluoride removal efficiency.

The XRD patterns of BC400, BCF_2M_1, and BCF_2M_1-F are presented in Fig. 7. All samples exhibited broad, diffuse background signals without distinct crystalline peaks, indicating the amorphous nature of the corncob biochar (Zhang L et al., 2023; Kumari N et al., 2024). This suggests that the biochar did not undergo graphitization during pyrolysis or Fe–Mn modification.

4. Conclusions

The main conclusions of this study are as follows:

(i) Addressing ecological health risks is a key focus of the United Nations Sustainable Development Goals. This study specifically examined the environmental risk posed by fluoride (F^-) contamination in groundwater.

(ii) Fe–Mn modified corncob biochar was successfully synthesized using an environmentally friendly and simple method involving $FeCl_3$ and $MnCl_2$. The modification significantly enhanced fluoride adsorption capacity due to the formation of Fe–O and Mn–O surface bonds, which facilitate complexation with F^-. SEM–EDS analysis revealed that BCF_2M_1 exhibited a rougher surface, more complex pore structure, and increased active sites for defluoridation. The fluoride removal mechanism involved heterogeneous, multi-layer, and physicochemical adsorption.

(iii) Fe–Mn coated corncob biochar is a low-cost, highly efficient, and environmentally sustainable material for fluoride remediation in soil and groundwater. This study highlights its potential for reducing fluoride pollution and improving water and soil quality in contaminated environments.

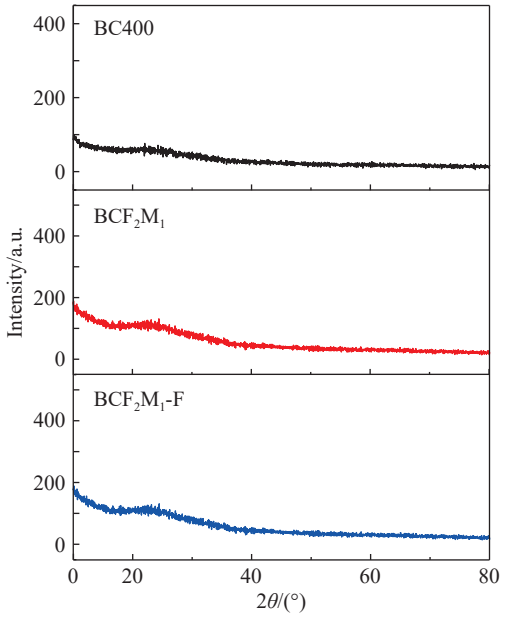

Fig. 7. XRD of corncob biochar before modification by Fe–Mn (BC400), after modified by Fe and Mn with the ratio of 1:2 (BCF_2M_1), and BCF_2M_1 after adsorbed F^- (BCF_2M_1-F).

CRediT authorship contribution statement

Juan-juan Liu conceived and planned the experiments. Wang-ying Chen and Si-yuan Ma contributed to sample preparation and the interpretation of the results. Juan-juan Liu wrote the manuscript with support from Xin-wen Yang and Abdur Rashid. Juan-juan Liu supervised the project. All authors provided critical feedback and helped shape the research, analysis, and manuscript.

Declaration of competing interest

The authors declare no conflicts of interest.

Acknowledgment

This research was financially supported by the National Natural Science Foundation of China (42007181), Chinese Academy of Geological Sciences Basal Research Fund (CSJ-2024-03), National Key Research and Development Program of China (2023YFC3709104). We also thank Shiyanjia (www.shiyanjia.com) for the support of XRD analysis.

Supplementary dataset

Supplementary data (Texts. S1-2, Table. S1, and Figure. S1) to this article can be found online at doi: 10.31035/cg20250075.

References

Ali S, Thakur SK, Sarkar A, Shekhar S. 2016. Worldwide contamination of water by fluoride. Environmental Chemisty Letters, 14, 291–315. doi: 10.1007/s10311-016-0563-5.

Borno ML, Muller-Stover DS, Liu F. 2018. Contrasting effects of biochar on phosphorus dynamics and bioavailability in different soil types. Science of the Total Environment, 627, 963–974. doi: 10.1016/j.scitotenv.2018.01.283.

Cheng J, Huang Y, Wang S, Miao L, Yan W. 2019. Transect variations and controlling factors of redox-sensitive trace element compositions of surface sediments in the South China Sea. Continental Shelf Research, 190, 103978. doi: 10.1016/j.csr.2019.103978.

Corona-Martinez DA, Díaz-Jiménez L, Reyes-Rosas A, Zermeño-González A, Samaniego-Moreno L, Khamkure S. 2025. Solvothermal synthesis of nanomagnetite-coated biochar for efficient arsenic and fluoride adsorption. Engineering Proceedings, 87, 67–73. doi: 10.3390/engproc2025087067.

Dewage NB, Liyanage AS, Pittman CU, Jr., Mohan D, Mlsna T. 2018. Fast nitrate and fluoride adsorption and magnetic separation from water on alpha-Fe_2O_3 and Fe_3O_4 dispersed on Douglas fir biochar. Bioresource Technology, 263, 258–265. doi: 10.1016/j.biortech.2018.05.001.

Foroutan R, Mohammadi R, Razeghi J, Ahmadi M, Ramavandi B. 2024. Amendment of Sargassum oligocystum bio-char with $MnFe_2O_4$ and lanthanum MOF obtained from PET waste for fluoride removal: A comparative study. Environmental Research, 251, 118641. doi: 10.1016/j.envres.2024.118641.

Foroutan R, Tutunchi A, Foroughi M, Ramavandi B. 2025. Efficient fluoride removal from water and industrial wastewater using magnetic chitosan_β-cyclodextrin aerogel enhanced with biochar and MOF composites. Separation and Purification Technology, 363, 132128. doi: 10.1016/j.seppur.2025.132128.

Freundlich. 1926. Colloid and Capillary Chemistry. Methuen and Co., Ltd., London, London.

Fu C, Zhou M, Song W, Yang G, Feng P, Chulalaksananukul W, Zhu S, Huang K, Wang Z. 2024. Innovative iron‐manganese modified microalgae biochar for efficient phosphate iron removal from water: Preparation and adsorption mechanisms. Journal of Water Process Engineering, 66, 106051. doi: 10.1016/j.jwpe.2024.106051.

GB7484-1987. 1987. Water quality-Determination of fluoride-Ion selective electrode method.

Girkar M, Shukla SP, Bharti V, Kumar K, Kumar S, Rathi Bhuvaneswari G. 2024. Removal of fluoride from groundwater by chemically functionalized sugarcane bagasse biochar and bagasse pellets in a fixed-bed sorption system. Desalination and Water Treatment, 317, 100044. doi: 10.1016/j.dwt.2024.100044.

Goswami R, Kumar M. 2018. Removal of fluoride from aqueous solution using nanoscale rice husk biochar. Groundwater for Sustainable Development, 7, 446–451. doi: 10.1016/j.gsd.2017.12.010.

Gourai M, Nayak AK, Nial PS, Satpathy B, Bhuyan R, Singh SK, Subudhi U. 2023. Thermal plasma processing of Moringa oleifera biochars: adsorbents for fluoride removal from water. RSC Advances, 13, 4340–4350. doi: 10.1039/d2ra07514h.

Guo J, Yan C, Luo Z, Fang H, Hu S, Cao Y. 2019. Synthesis of a novel ternary HA/Fe-Mn oxides-loaded biochar composite and its application in cadmium(II) and arsenic(V) adsorption. Journal of Environmental Science, 85, 168–176. doi: 10.1016/j.jes.2019.06.004.

He J, Yang Y, Wu Z, Xie C, Zhang K, Kong L, Liu J. 2020. Review of fluoride removal from water environment by adsorption. Journal of Environmental Chemical Engineering, 8, 104516. doi: 10.1016/j.jece.2020.104516.

Ho YS. 2006. Review of second-order models for adsorption systems. Journal of Hazardous Materials, 136, 681–689. doi: 10.1016/j.jhazmat.2005.12.043.

Hota A, Patro SGK, Panda SK, Khan MA, Hasan MA, Islam S, Alsubih M, Khan NA, Zahmatkesh S. 2024. Removing fluoride ions from wastewater by Fe_3O_4 nanoparticles: Modified Rhodophytes (red algae) as biochar. Journal of Water Process Engineering, 58, 104776. doi: 10.1016/j.jwpe.2024.104776.

Khan BA, Ahmad M, Iqbal S, Bolan N, Zubair S, Shafique MA, Shah A. 2022. Effectiveness of the engineered pinecone-derived biochar for the removal of fluoride from water. Environmental Research, 212, 113540. doi: 10.1016/j.envres.2022.113540.

Kumar R, Sharma P, Rose PK, Sahoo PK, Bhattacharya P, Pandey A, Kumar M. 2023. Co-transport and deposition of fluoride using rice husk-derived biochar in saturated porous media: Effect of solution chemistry and surface properties. Environmental Technology & Innovation, 30, 103056. doi: 10.1016/j.eti.2023.103056.

Kumar R, Sharma P, Sharma PK, Rose PK, Singh RK, Kumar N, Sahoo PK, Maity JP, Ghosh A, Kumar M, Bhattacharya P, Pandey A. 2023. Rice husk biochar-A novel engineered bio-based material for transforming groundwater-mediated fluoride cycling in natural environments. Journal of Environmental Management, 343, 118222. doi: 10.1016/j.jenvman.2023.118222.

Kumari N, Marandi S, Pandey S. 2024. Fluoride removal from groundwater using fish scales derived biochar. Materials Today: Proceedings. doi:10.1016/j.matpr.2024.01.033.

Lacson CFZ, Lu MC, Huang YH. 2021. Fluoride-containing water: A global perspective and a pursuit to sustainable water defluoridation management -An overview. Journal of Cleaner Production, 280, 124236. doi: 10.1016/j.jclepro.2020.124236.

Langmuir I. 1917. The constitution and fundamental properties of solids and liquids. Journal of the Franklin Institute, 183, 102–105. doi: 10.1016/S0016-0032(17)90938-X.

Li FY, Jiang TY, Yu T, Yang ZF, Hou QY, Wang LX. 2021. Review on sources of fluorine in the environment and health risk assessment. Rock and Mineral Analysis, 40(6), 793–807 (in Chinese with English abstract). doi: 10.15898/j.cnki.11-2131/td.202109290133.

Li YX, Chen JY, Han R, Luan RJ, Zhang YQ, Wu LD, Qi ZC. 2023. Effects of phosphate on the adsorption of heavy metal Ions onto TiO2 nanoparticles in water and mechanism analysis. Rock and Mineral Analysis, 42(2), 317–325 (in Chinese with English abstract). doi: 10.15898/j.cnki.11-2131/td.202206170114.

Li J, Guo Z, Cui K, Chen X, Yang X, Dong D, Xi S, Wu Z, Wu F. 2023. Remediating thiacloprid-contaminated soil utilizing straw biochar-loaded iron and manganese oxides activated persulfate: Removal effects and soil environment changes. Journal of Hazardous Materials, 459, 132066. doi: 10.1016/j.jhazmat.2023.132066.

Lin L, Qiu W, Wang D, Huang Q, Song Z, Chau HW. 2017. Arsenic removal in aqueous solution by a novel Fe-Mn modified biochar composite: Characterization and mechanism. Ecotoxicology and Environmental Safety, 144, 514–521. doi: 10.1016/j.ecoenv.2017.06.063.

Liu H, Liu Y, Tang L, Wang J, Yu J, Zhang H, Yu M, Zou J, Xie Q. 2020. Egg shell biochar-based green catalysts for the removal of organic pollutants by activating persulfate. Science of the Total Environment, 745, 141095. doi: 10.1016/j.scitotenv.2020.141095.

Liu JJ, Gao XB, Dai C, Zhang SN, Kong SQ, Wang L, Hu YD. 2025. Cr(III)-incorporated Fe(III) hydroxides for enhanced redox conversion of As(III) and Cr(VI) in acidic solution. Environmental Science: Nano, 12, 2064–2075 doi: 10.1039/d4en01068j.

Liu JJ, Wu XL, Hu YD, Dai C, Peng Q, Liang DL. 2016. Effects of Cu(II) on the adsorption behaviors of Cr(III) and Cr(VI) onto Kaolin. Journal of Chemistry, 2016, 1–11. doi: 10.1155/2016/3069754.

Mahdavi Z, Peighambardoust SJ, Foroughi M, Foroutan R, Ahmadi M, Ramavandi B. 2024. Enhancing fluoride ion removal from aqueous solutions and glass manufacturing wastewater using modified orange peel biochar magnetic composite with MIL-53. Environmental Research, 262, 119825. doi: 10.1016/j.envres.2024.119825.

Mei L, Qiao H, Ke F, Peng C, Hou R, Wan X, Cai H. 2020. One-step synthesis of zirconium dioxide-biochar derived from Camellia oleifera seed shell with enhanced removal capacity for fluoride from water. Applied Surface Science, 509, 144685. doi: 10.1016/j.apsusc.2019.144685.

Meilani V, Lee J-I, Kang J-K, Lee C-G, Jeong S, Park S-J. 2021. Application of aluminum-modified food waste biochar as adsorbent of fluoride in aqueous solutions and optimization of production using response surface methodology. Microporous and Mesoporous Materials, 312, 110764. doi: 10.1016/j.micromeso.2020.110764.

Mohan D, Kumar S, Srivastava A. 2014. Fluoride removal from ground water using magnetic and nonmagnetic corn stover biochars. Ecological Engineering, 73, 798–808. doi: 10.1016/j.ecoleng.2014.08.017.

Mohan D, Sharma R, Singh VK, Steele P, Pittman CU. 2012. Fluoride removal from water using bio-char, a green waste, low-cost adsorbent: Equilibrium uptake and sorption dynamics modeling. Industrial & Engineering Chemistry Research, 51, 900–914. doi: 10.1021/ie202189v.

Montero JIZ, Monteiro ASC, Gontijo ESJ, Bueno CC, de Moraes MA,

Rosa AH. 2018. High efficiency removal of As(III) from waters using a new and friendly adsorbent based on sugarcane bagasse and corncob husk Fe-coated biochars. Ecotoxicology and Environmental Safety, 162, 616–624. doi: 10.1016/j.ecoenv.2018.07.042.

Mwadalu R, Rutto M, Abdi AM, Chappa LR, Nungula EZ, Ngaiza VV, Raj A, Dlamini JC, Raza MA, Soratto RP, Nasar J, Gitari HI, 2025. Potential of biochar for defluoridation of drinking water: A review. in: Sharma K (Ed.). Fluorides in drinking water. Environmental Science and Engineering. Springer. 143–161. doi:10.1007/978-3-031-77247-4_6.

Ning K, Chen H, Wang D, Hu Y, He Y, Hao S, Cui Q, Zheng S. 2024. Effective removal of fluoride and lead ions from aqueous solutions using water treatment residue and rice straw co-pyrolysis biochar composites. Environmental Technology & Innovation, 34, 103589. doi: 10.1016/j.eti.2024.103589.

Rasool A, Farooqi A, Xiao T, Ali W, Noor S, Abiola O, Ali S, Nasim W. 2018. A review of global outlook on fluoride contamination in groundwater with prominence on the Pakistan current situation. Environmental Geochemistry and Health, 40, 1265–1281. doi: 10.1007/s10653-017-0054-z.

Sadhu M, Bhattacharya P, Vithanage M, Padmaja Sudhakar P. 2021. Adsorptive removal of fluoride using biochar – A potential application in drinking water treatment. Separation and Purification Technology, 278, 119106. doi: 10.1016/j.seppur.2021.119106.

Wan S, Lin J, Tao W, Yang Y, Li Y, He F. 2019. Enhanced fluoride removal from water by nanoporous biochar-supported magnesium oxide. Industrial & Engineering Chemistry Research, 58, 9988–9996. doi: 10.1021/acs.iecr.9b01368.

Wang BL, Zhang YJ, Zhang YH, Chen Y. 2024. Research progress of biochar based materials and their applications using electrochemical sensors. Rock and Mineral Analysis, 43(6), 967–981 (in Chinese with English abstract). doi: 10.15898/j.ykcs.202403170058.

Wang J, Zhu H, Hu Y, Hu L, Wei Z, Li YY, Hu X. 2025. Mn oxide-modified biochars with high adsorption capacity for Pb(II) in wastewater: Preparation and adsorption mechanisms. Environmental Research, 266, 120553. doi: 10.1016/j.envres.2024.120553.

Wang Y, Ji H, Lyu H, Liu Y, He L, You L, Zhou C, Yang S. 2019. Simultaneous alleviation of Sb and Cd availability in contaminated soil and accumulation in Lolium multiflorum Lam. After amendment with Fe–Mn-modified biochar. Journal of Cleaner Production, 231, 556–564. doi: 10.1016/j.jclepro.2019.04.407.

Yang T, Xu Y, Huang Q, Sun Y, Liang X, Wang L. 2022. Removal mechanisms of Cd from water and soil using Fe-Mn oxides modified biochar. Environmental Research, 212, 113406. doi: 10.1016/j.envres.2022.113406.

Yang MG, Sun H, Cao HL, Jia ZH, Feng ZY, Zheng LJ, Chen N. 2023. Preparation and application of biochar-chitosan magnetic composite adsorbent for removal of lead and copper from groundwater. Rock and Mineral Analysis, 42(3), 563–575 (in Chinese with English abstract). doi: 10.15898/j.ykcs.202208230155.

Yang YZ, Gao BL, Huang Y, Xiao DC, Chen F, Luo H, Li LF, Wu G. 2023. The adsorption characteristics of Pb^{2+} and Cd^{2+} by straw based biochars generated at medium-high pyrolysis temperatures. Geology in China, 50(1), 52–60 (in Chinese with English abstract). doi: 10.12029/gc20220509001.

Yin G, Song X, Tao L, Sarkar B, Sarmah AK, Zhang W, Lin Q, Xiao R, Liu Q, Wang H. 2020. Novel Fe-Mn binary oxide-biochar as an adsorbent for removing Cd(II) from aqueous solutions. Chemical Engineering Journal, 389, 124465. doi: 10.1016/j.cej.2020.124465.

Zhang L, Hu J, Li C, Chen Y, Zheng L, Ding D, Shan S. 2023. Synergistic mechanism of iron manganese supported biochar for arsenic remediation and enzyme activity in contaminated soil. Journal of Environmental Management, 347, 119127. doi: 10.1016/j.jenvman.2023.119127.

Zou CJ, Shi ZM, Zhang N, Zhu YH, Yang LH, Wang XY. 2024. Synergistic effects of potassium-silicon-calcium mineral fertilizer combined with rice husk biochar on the immobilization of Cd and Pb in soil. China Geology, 7, 1–12. doi: 10.31035/cg20230050.